SAND2017-12637R

Heavy-Duty Low-Temperature and Diesel Combustion & Heavy-Duty Combustion Modeling

Mark PB Musculus, Principal Investigator
Organization: Sandia National Laboratories
Address:
PO Box 969, MS 9053
Livermore, CA 94551-0969
Phone: (925) 294-3435
E-mail: mpmuscu@sandia.gov

Gurpreet Singh, DOE Program Manager
U.S. Department of Energy
Phone: (202) 586-2333
E-mail: gurpreet.singh@ee.doe.gov

Start Date: October 1, 2016 End Date: September 30, 2017
Total Project Cost: $580k DOE share: $580k Non-DOE share: $0

Project Introduction

Regulatory drivers and market demands for lower pollutant emissions, lower carbon dioxide emissions, and lower fuel consumption motivate the development of clean and fuel-efficient engine operating strategies. Most current production engines use a combination of both in-cylinder and exhaust emissions-control strategies to achieve these goals. The emissions and efficiency performance of in-cylinder strategies depend strongly on flow and mixing processes associated with fuel injection.

Various diesel engine manufacturers have adopted close-coupled post-injection combustion strategies to both reduce pollutant emissions and to increase engine efficiency for heavy-duty applications, as well as for light- and medium-duty applications. Close-coupled post-injections are typically short injections that follow a larger main injection in the same cycle after a short dwell, such that the energy conversion efficiency of the post-injection is typical of diesel combustion. Of the various post-injection schedules that have been reported in the literature, effects on exhaust soot vary by roughly an order of magnitude in either direction of increasing or decreasing emissions relative to single injections (O'Connor et al., 2015). While several hypotheses have been offered in the literature to help explain these observations, no clear consensus has been established. For new engines to take full advantage of the benefits that post-injections can offer, the in-cylinder mechanisms that affect emissions and efficiency must be identified and described to provide guidance for engine design.

Objectives

This project includes diesel combustion research at Sandia National Laboratories (SNL) and combustion modeling at the University of Wisconsin (UW). The overall objectives are:

- Develop fundamental understanding of how in-cylinder controls can improve efficiency and reduce pollutant emissions of advanced low-temperature combustion (LTC) technologies
- Quantify the effects of fuel injection, mixing, and combustion processes on thermodynamic losses and pollutant emission formation
- Improve computer modeling capabilities to accurately simulate these processes

Fiscal Year (FY) 2017 Objectives

- Measure how in-cylinder soot and/or soot precursor formation are affected by in-cylinder conditions and processes
- Use computer model simulations to complement experimental soot and spray data to provide a deeper mechanistic understanding of in-cylinder processes

Approach

This project uses an optically-accessible, heavy-duty, direct-injection diesel engine (Figure 1). A large window in the piston crown provides primary imaging access to the piston bowl, and other windows at the cylinder wall provide cross-optical access for laser diagnostics or imaging.

The optical setup in Figure 1 uses two cameras to record simultaneous images of soot natural luminosity (NL) and diffused back-illumination (DBI) soot extinction. DBI measures the soot optical density through light transmission measurements, and mitigates beam-steering effects by using a diffused light source. The light source is a 632-nm pulsed light-emitting diode (LED) in the top-right corner of Figure 1. The LED emission is collimated using two lenses and a pinhole, after which the beam is directed down onto an engineered diffuser, through a cylinder-head window, the combustion chamber with soot, and piston crown window. Thereafter, a beamsplitter directs most of the beam to a high-speed complementary metal-oxide semiconductor (CMOS) camera, while a second high-speed CMOS camera captures NL simultaneously.

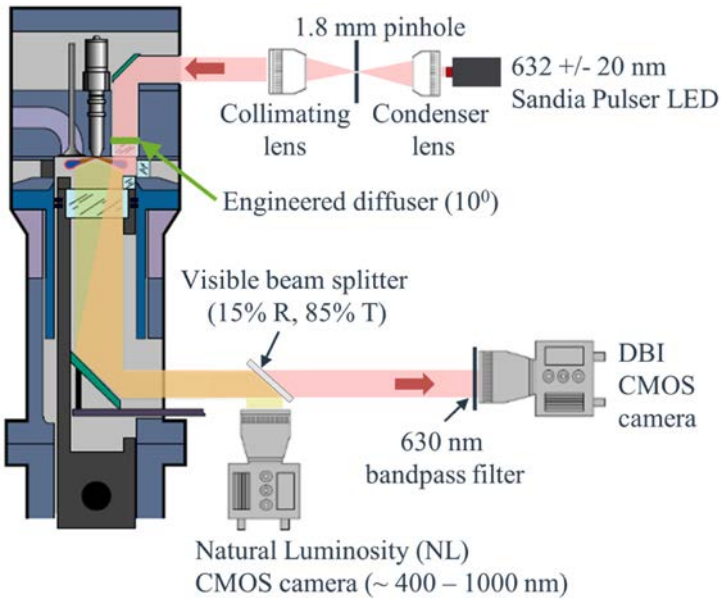

Figure 1. Optical engine schematic showing LED beam path (propagating from top to bottom) and two-camera setup for simultaneous DBI and NL imaging.

Results

Figure 2 shows the dependence of the paper-blackening (PB) measurement of engine-out smoke emission on the gross indicated mean effective pressure (IMEPg) for various single-injection and post-injection schedules, all with the same 347 crank-angle degree (CAD, where 360 is at end of compression) start of solenoid energizing (SSE) of the main injection, but different main-injection duration of solenoid energizing (DSE) and/or different post-injection SSE and DSE. Operating conditions use nitrogen dilution to 18% intake O_2 and the estimated thermodynamic conditions at top-dead center (TDC) for a motored charge are 15.8 kg/m^3 and 910 K. The blue trendline for single-injection operating conditions shows monotonically increasing PB with increasing main-injection DSE. The addition of post injections of up to 550 µs DSE to the main injection (with a constant 2350 µs DSE) does not increase the measured PB. A post injection of 600 µs DSE increases the PB relative to the main injection alone, but the PB remains lower than the single-injection PB trend at the same load and SSE. As the post-injection DSE is increased to 800 µs, the PB exceeds the single-injection PB trend at the same load.

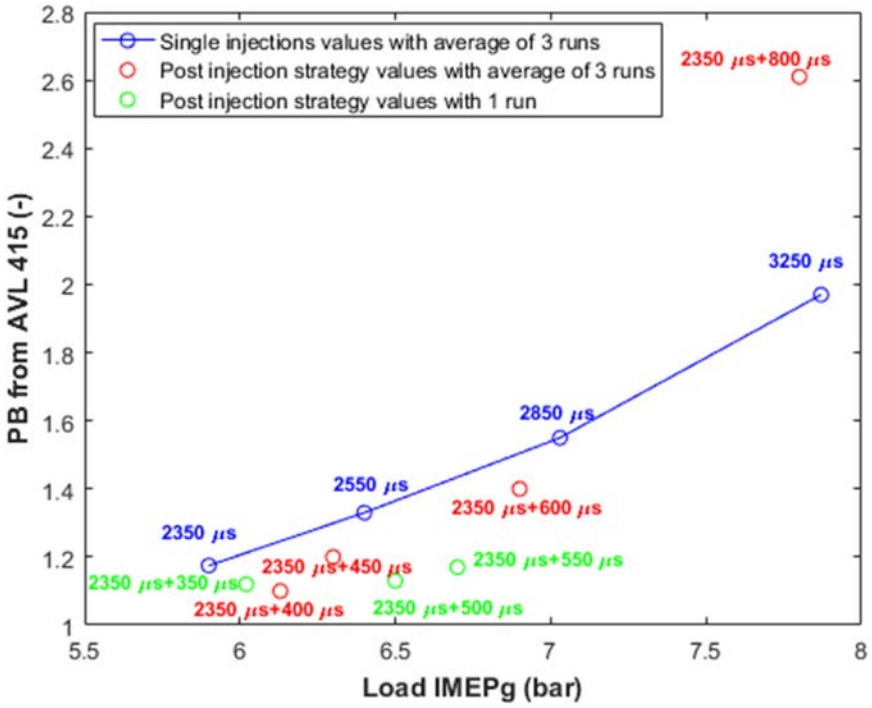

Figure 2. Mean PB for using various single- and post-injection schedules. 18% intake O_2, 15.8 kg/m^3 and 910 K TDC motored.

Insight into the in-cylinder mechanisms responsible for the engine-out emissions behavior in Figure 2 may be gained through analysis of the in-cylinder imaging data. Figure 3 shows crank-angle-resolved soot optical density on a natural-logarithmic scale (KL), averaged over the DBI field of view (FoV) for a reference single-injection and selected post-injection operating conditions in Figure 2. The KL data in Figure 3 show two peaks. The left-hand peak is from the main injection, while the right-hand peak is due to the post-injection, the height of which depends on the DSE of the post injection. The 400-µs DSE post injection (green line) has a minimal effect relative to the single injection data, but larger post-injection DSEs show increasing departures from the single-injection data. The 800-µs DSE post injection (magenta line) has the highest peak KL, even higher than the main injection peak. The late-cycle KL (far right in Figure 3, when cylinder contents are well-mixed) also follows the exhaust emissions trends in Figure 2, with the longer post-injections having higher late-cycle KL (Figure 3) and engine-out PB (Figure 2) than shorter post-injections. Indeed, Figure 4 shows that the correlations between late-cycle KL and engine-out PB for the data in Figure 2 is quite good (R-squared of 0.968).

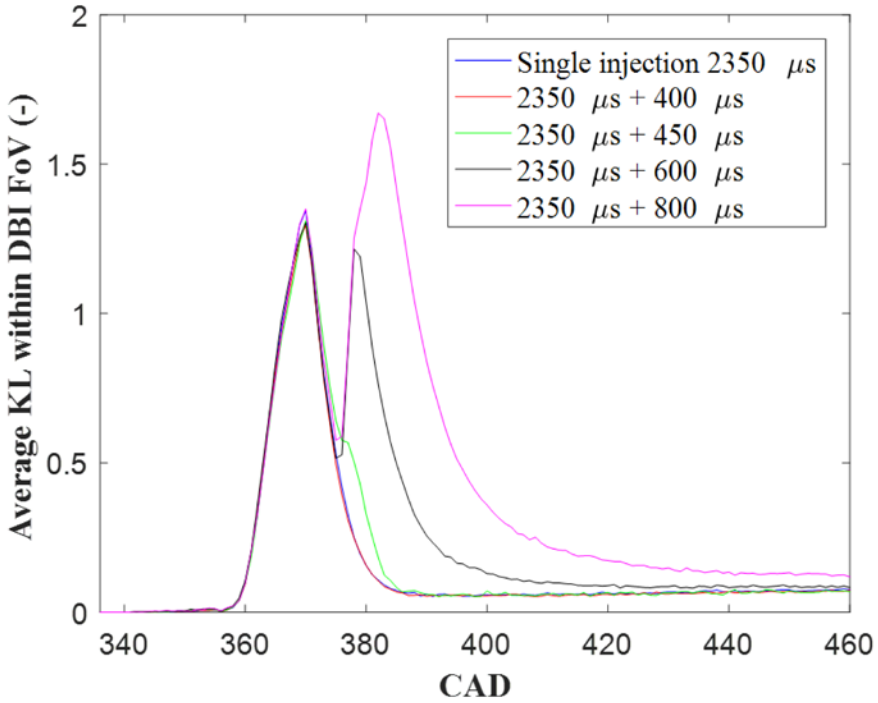

Figure 3. KL evolution within the DBI FoV from ensemble-averaged images with post-injections of various DSE added to a main injection of 2350 μs DSE, as indicated in the legend. 18% intake O_2, 15.8 kg/m^3 and 910 K TDC motored.

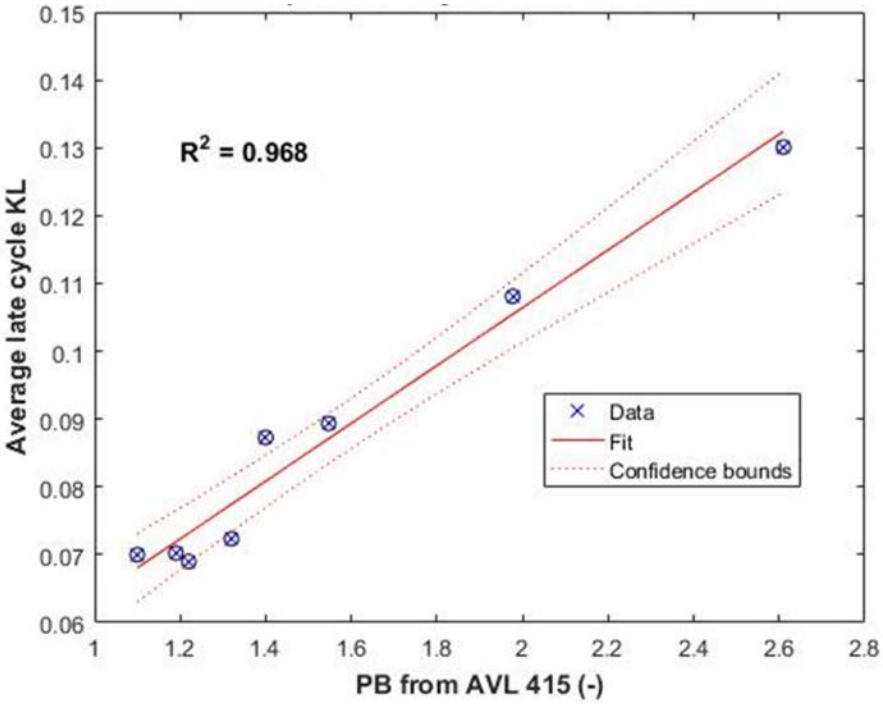

Figure 4. Correlation between the late-cycle FoV-averaged KL and engine-out PB data in Figure 2 that have three replicates. Dotted lines show the 95% confidence interval.

Further insight into the in-cylinder processes by which post injections affect in-cylinder and engine-out soot may be gained by comparing the KL and NL images. Figure 5 is a composite graphic comparing ensemble-averaged KL and NL data at one point in the cycle for two different conditions, one with a single injection and one with a load-equivalent post-injection (see injector solenoid energizing schedule in top-left of Figure 5). The piston and spray geometry at the selected image timing of 379 CAD (with TDC of compression at 360 CAD) is shown in the bottom left of Figure 5. The top row of images are false-colored according to the DBI-measured soot KL for the single (left) and main+post (middle) injection schedules, and the difference between the two (right). Similarly, the bottom row shows corresponding NL images. The NL images show a partial view of the piston bowl, with the injector at the bottom-right, and the piston bowl forming the outer circle. The curved white line shows the FoV of the DBI images. The KL difference image at the top-right shows that the amount of soot (KL) is increased in some locations (green) and is decreased in others, while the NL difference image in the bottom right shows a different pattern. Of particular interest are the two regions identified by the red dots with connecting lines showing opposite trends in the KL and NL data. Both the KL and the NL increase near the upper-right dot pair in each image, while the KL decreases and the NL increases for the lower-left dot pair. The NL signal increases with both temperature and the amount of soot, and the KL data shows that the amount of soot decreases in the vicinity of the lower-left dot, which implies that the temperature must increase when the post-injection is added for the NL signal to increase. This provides in-cylinder evidence for a mechanism of soot reduction by increasing local temperatures, which should enhance local soot oxidation. This same mechanism was suggested by previous soot PLII and OH PLIF imaging data from this project (Musculus, 2014), and the current temperature data further strengthen these indications of previous work regarding the in-cylinder mechanisms by which post-injections affect in-cylinder soot. Later in the cycle (not shown here), the KL difference data show lower KL after the post injection, which is consistent with the action of a second entrainment wave for the post injection that increases entrainment to aid soot oxidation, as shown in previous work on this project (Musculus, 2008).

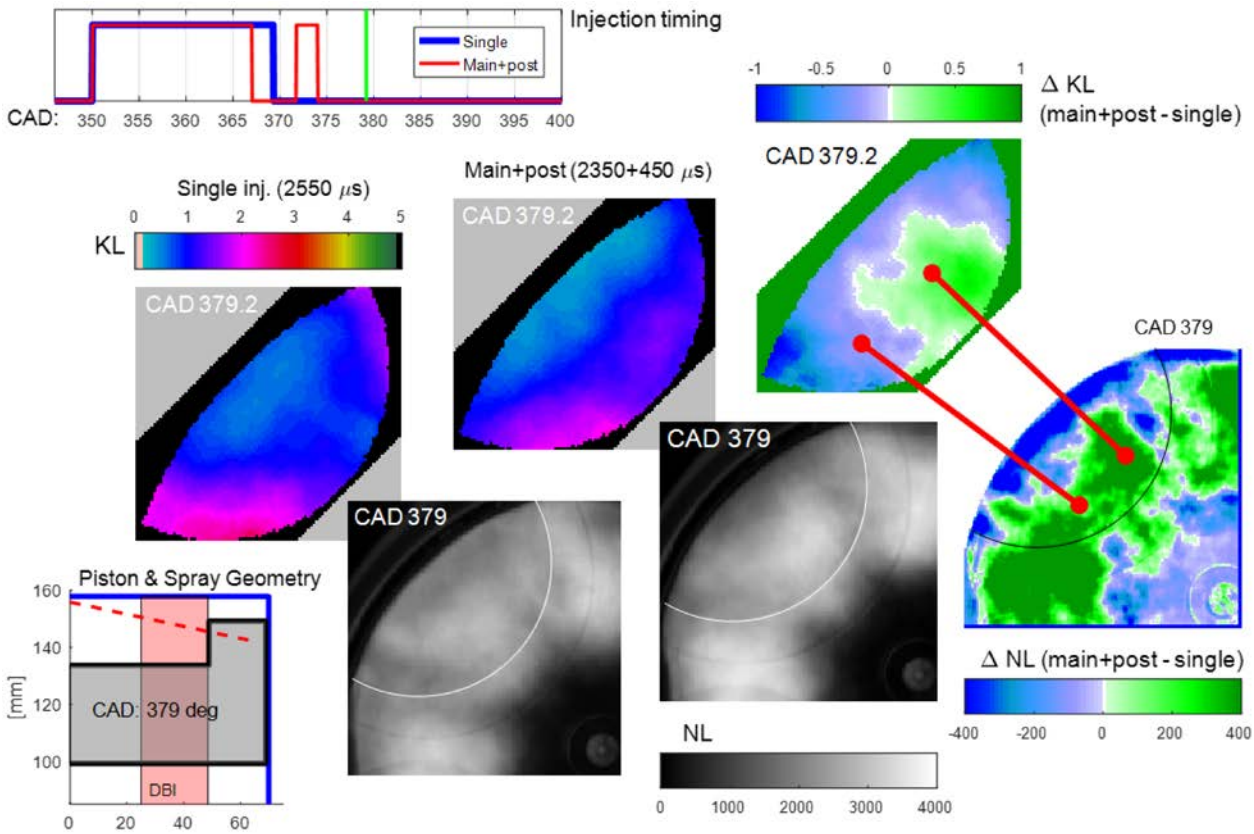

Figure 5. Composite graphic showing injector solenoid energizing schedule (top-left), in-cylinder geometry (bottom-left), soot KL measured by ensemble-averaged

DBI (top row of images) and ensemble-averaged soot NL (bottom row of images). Each KL and NL row shows images with the single injection only (left), a load-equivalent schedule with a post-injection (middle) and a false-colored image of the difference in between the post- and single-injection images. The red dots and lines identify regions that are discussed in the text.

Finally, computer modeling simulations provide additional insight into these NL/KL comparisons. Figure 6 illustrates how the two-dimensional (2D) NL images measured in the experiments can be predicted from the three-dimensional (3D) in-cylinder soot distributions from the simulations. The top row shows a comparison of a measured 2D NL image (left) with a predicted 2D NL image (middle), which is based on the predicted 3D soot distribution (right). The equation at the top of Figure 6 shows how the soot volume-fraction-path-length product (f_vL), which is related to KL, can be converted to NL using a base-ten transfer function with a variable exponent (tf). The bottom row shows that a static transfer-function map overlaid on the experimental image (left) can be applied to estimate the fvL (middle), which agrees well with the simulation predictions (right).

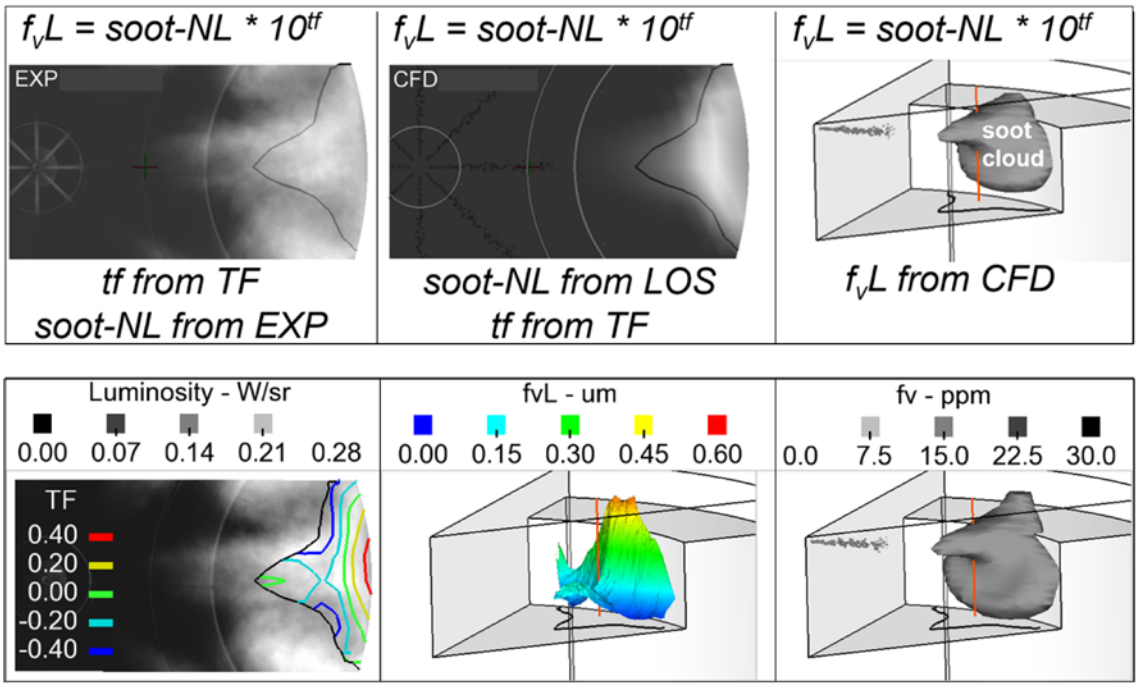

Figure 6. Top row: measured 2D NL image (left), predicted 2D NL image (right), predicted 3D soot distribution (right). Bottom row: transfer function map overlaid on measured NL (left), estimated experimental f_vL (middle) and predicted 3D f_v distribution.

Conclusions

- New combined DBI and NL imaging technique shows first clear evidence of post-injection soot reduction by increased local temperatures, strengthening suggestions from 2014 soot PLII and OH PLIF imaging data (Musculus, 2014)
- Quantitative soot DBI imaging shows late-cycle reduction of soot in post-jet, consistent with increased mixing from a second entrainment wave, a new fluid-mechanic effect that was described in 2008 (Musculus, 2008)
- Developed soot volume fraction (fvL) to NL transfer function to aid interpretation of NL images

References

O'Connor J, Musculus MPB, "Post injections for soot reduction in diesel engines: a review of current understanding," SAE Int. J. Engines 6(1):400-421, 2013

Musculus MPB, "Heavy-duty low-temperature and diesel combustion & heavy-duty combustion modeling," FY 2008 DOE Hydrogen & Fuel Cells Program and Vehicle Technologies Program Annual Merit Review and Peer Evaluation Meeting, Advanced Combustion Engine R&D/Combustion Research, 2008

Musculus MPB, "Heavy-duty low-temperature and diesel combustion & heavy-duty combustion modeling," FY 2014 DOE Hydrogen & Fuel Cells Program and Vehicle Technologies Program Annual Merit Review and Peer Evaluation Meeting, Advanced Combustion Engine R&D/Combustion Research, 2014

Key Fiscal Year 2017 Publications

1. "Influence of injection duration and ambient temperature on the ignition delay in a 2.34L optical diesel engine," Malbec LM, Eagle WE, Musculus MPB and Schihl P, SAE Int. J. Engines 9:47-70, April 2016.
2. "Measurements of liquid length, vapor penetration, ignition delay, and flame lift-off length for the Engine Combustion Network `Spray~B' in a 2.34L Optical Heavy-Duty Diesel Engine," W.E. Eagle, L-M. Malbec, M.P.B. Musculus, SAE Int. J. Engines 9:910-931, June 2016.
3. "An improved entrainment rate measurement method for transient jets from 10kHz particle image velocimetry," WE Eagle, MPB Musculus, L-MC Malbec, G Bruneaux, accepted to Atomization and Sprays, July 2016.
4. "Effect of post injections on mixture preparation and unburned hydrocarbon emissions in a heavy-duty diesel engine," J. O'Connor, M. Musculus, L. Pickett, Combustion and Flame 170:111-123, August 2016.
5. "Optical imaging to understand fuel reactivity effects on RCCI combustion," WE Eagle, MPB Musculus, AEC Meeting, Detroit MI, August 2016.
6. "On using diffuse back-illuminated imaging for soot extinction measurements within an optically accessible heavy-duty diesel engine," G Roberts, MPB Musculus, AEC Meeting, Detroit MI, August 2016.
7. "Recent research toward the co-optimization of fuels and engines," FISITA 2016 World Automotive Congress, Busan, South Korea, September 2016.
8. "Infrared emission detection as a fuel-vapor penetration diagnostic," Thiesel Conference poster, Valencia Spain, September 2016.
9. "The co-optimization of fuels and engines: chemical kinetics and optical research," MPB Musculus, Lund University, Sweden, October 2016.
10. "Quantitative assessment of in-cylinder soot reduction mechanisms of post injections," G Roberts, MPB Musculus, AEC Meeting, USCAR, Southfield, MI, January, 2017.
11. "The in-cylinder intersection of thermofluids and chemistry as revealed by optical diagnostics," MPB Musculus, Thermal and Fluid Sciences Functional Excellence (TSFE) Conference, Cummins Tech Center, Columbus IN, April 4, 2017.
12. "Guidelines for interpreting soot luminosity imaging," RP Hessel, Z Yue, RD Reitz, MPB Musculus, JA O'Connor, SAE Int. J. Engines 10(3), 2017.
13. "Comparing infrared emission from hydrocarbon C-H stretch during direct injection with and without reaction in an optical heavy duty engine," WE Eagle, G Roberts, MPB Musculus, L-M Malbec, L Sequino, E Mancaruso, 10th U. S. National Combustion Meeting, College Park, Maryland, April 23-26, 2017.

Acronyms, Abbreviations, Symbols, & Units

2D	Two Dimensional
3D	Three Dimensional
CAD	Crank Angle Degrees (for position, with 360 = TDC compression)
CMOS	Complementary Metal Oxide Semiconductor (camera)
DBI	Diffused Background Illumination
DSE	Duration of Solenoid Energizing
FoV	Field of View

f_vL	Soot volume-fraction-path-Length product
FY	Fiscal Year
IMEPg	Indicated Mean Effective Pressure, gross
KL	Soot optical density on natural-logarithmic scale
LED	Light-Emitting Diode
LTC	Low-Temperature Combustion
NL	Natural Luminosity (soot)
PB	Particulate Blackening (exhaust smoke measurement)
SNL	Sandia National Laboratories
SSE	Start of Solenoid Energizing
TDC	Top-Dead Center
tf	transfer function exponent
UW	University of Wisconsin